Alma Mater Studiorum Università di Bologna
Archivio istituzionale della ricerca

Cascaded Rectifiers for Energy Harvesting With a Wide Dynamic Power Range

(Article begins on next page)

06 May 2024

Cascaded Rectifiers for Energy Harvesting with a Wide Dynamic Power Range

S. Trovarello, *Student Member, IEEE*, G. Paolini, *Member, IEEE*, D. Masotti, *Senior Member, IEEE*, and A. Costanzo, *Fellow, IEEE*

Abstract— **This work presents a novel RF energy harvesting system at 2.45 GHz, operating over a wide dynamic RF range (44 dB), starting from ultra-low power. It consists of three rectification branches, each one optimized for a selected power interval, between -20 ÷ +24 dBm. Through an automatic distribution network, the incident RF power is routed to the most efficient rectification branch, with no need for external control circuits. The first branch is optimized for low-power conditions, in the range -20 ÷ 0 dBm, and the second and third branches for 0 ÷ 9 dBm and 9 ÷ 24 dBm, respectively. For branch decoupling, an original strategy, based on the concurrent nonlinear design of power-dependent matching networks and self-powered switches, is used. To maximize each rectifier performance, Enhancement-mode High Electron Mobility transistors (HEMT) are adopted by means of the self-biasing mechanism. In this way, for any possible incoming RF power, only the most suitable rectifier path is active and the maximum RF-to-dc conversion efficiency is preserved. The system has been fabricated and tested demonstrating a conversion efficiency higher than 30% from -13 dBm to 24 dBm, with the lowest and highest measured dc output voltage of 0.1 and 13 V, respectively.**

Index Terms—**energy harvesting, harmonic balance, HEMT, nonlinear simulation, radiofrequency, rectifier.**

I. INTRODUCTION

THE use of radiofrequency (RF) power to harvest energy has stimulated a lot of interest in recent years thanks to low costs and ease of manufacturing [1].

In general, most electronic devices are supplied with batteries. This type of configuration implies additional costs due to the accumulator, larger dimensions to house the latter, and regular maintenance for ensuring the operations of the device. RF energy harvesting (EH) is therefore proposed as a solution to this series of issues by converting the RF energy, received through the wireless link, into dc.

One of the most promising candidates, for exploiting RF EH, are the wireless sensor networks (WSN), which are generally composed of a large number of sensors with low power consumption requirements [2], [3]. Sensor networks with are increasingly adopted in many applications, such as predictive maintenance, supply chain monitoring, tracking,

Simone Trovarello, Giacomo Paolini, Diego Masotti, and Alessandra Costanzo are with DEI "Guglielmo Marconi", University of Bologna, Bologna 40136, Italy (e-mail:simone.trovarello2@unibo.it, giacomo.paolini4@unibo.it, diego.masotti@unibo.it, alessandra.costanzo@unibo.it).

and surveillance, among others [4]. In all these applications, one of the key requirement is to keep the sensors alive as much as possible [5-7]. Furthermore, for remote structural monitoring or wearable or implanted biomedical systems [8] it is needed to operate without the aid of maintenance, given the difficulty in reaching the sensors themselves. RF EH systems have therefore encountered increasing interest in recent years thanks to their potential in solving this issue.

RF rectification systems usually adopt a single rectenna, whose circuital parameters are optimized using harmonic balance-based computer-aided design (CAD) methods and exhibit optimal performance only for a prescribed power range. Consequently, they can be effectively exploited when the received power is well defined and almost constant or within a limited range.

However, in most of the application environments of interest, such as indoor ones, the received power is not constant and easy to be predicted but depends on several factors, such as the distance from the transmitter and its polarization, the radio channel, and the surrounding environment. Therefore, it becomes essential to rely on wide-dynamic-range rectification systems in such a way to always take advantage of the best RF-to-dc conversion efficiency. The key idea is to seamlessly combine multiple rectifiers, each one optimized to operate over a prescribed power range, depending on the current availability of RF power.

Many solutions have been presented in the literature to convey the power flow to the most suitable rectifier, but many of those rely on an external control unit. In the approach proposed in [8], a three-stage rectifier, based on single pole double throw (SPDT), is presented. In this work, the input RF signal is branched by a directional coupler, driven by a power monitoring unit that controls the rectifiers selection through two SPDT switches. Three rectifiers, operating for different power levels, are alternatively selected by an external control unit and the system efficiently operates over a wide dynamic range (from 5 to 45 dBm). However, the minimum needed power is quite high, and it is partly used to support the controller and the power monitoring system, since the SPDT is controlled by a monitor consisting of a central processing unit (CPU) and a power detector which not only consumes power but also significantly increases the overall cost and size of the EH system.

In [9], [10], and [11] instead, an adaptive matching technique is adopted: for each rectifier branch, a nonlinear

optimization is carried out to obtain antenna-to-rectifier networks strongly selective for the prescribed input power range: in this way, it is possible to convey the power flow to the most suitable rectifier, disfavoring its flow to the unsuitable ones. Good peak efficiencies have been demonstrated in [9] (60%), [10] (81%), and [11] (60%), with a dynamic range of 29 dB, 40 dB, and 40 dB, respectively, but starting from a quite high minimum power level. Indeed, to the authors' knowledge, none of the solutions currently available can work efficiently for ultra-low power conditions.

Furthermore, in [11], each rectification branch has its own resistive load, while the power conversion efficiency (PCE) of the multi-branch system is calculated considering the sum of all the rectified power from the branches, which clearly leads to higher efficiencies, but cannot be exploited unless a multi-input PMU is used. Moreover, in the abovementioned work, the rectification starts from a minimum input power of -15 dBm, which entails not exploiting lower power values, which indeed can occur in dynamic environments. Furthermore, in solutions of the kind of [11], decoupling among stages is not controlled. In this way, if the input power rises, it can damage the low-power stage, if the diode experiences the breakdown voltage. An interesting alternative is presented in [12], where the rectifier circuit adopts a zero-threshold enhancement-mode high-electron-mobility transistor (HEMT) and the transistor is kept in its high-efficiency operating region by a suitable embedded circuit which generates the needed negative dc gate-source voltage (V_{GS}), for tracking optimum efficiency. In this way, a 44-dB dynamic range is demonstrated but a low RF-to-dc efficiency for low input power levels (13% at -20 dBm) is observed.

This work proposes an alternative system of rectifiers, to cover dynamic power ranges larger than 40 dB, starting from RF powers as low as -20 dBm. At these power levels, such a low conversion efficiencies have been demonstrated that make the use of the energy harvesting system useless.

The architecture proposed in this work, consists of the parallel connection of three rectifier branches, each one optimized for a specific power range: in the following they will be referred as low-power (LPR), medium-power (MPR), and high-power (HPR) rectifiers, respectively. They are seamlessly and alternately activated, depending on the incoming RF power only, without the need for any external control. This is the peculiar aspect of the present solution which is obtained by connecting the RF input port directly to the LPR, whereas the MPR and HPR ones are connected through a floating-gate unbiased HEMT. Enhanced-mode HEMTs have been selected because they guarantee ports isolation [13] and do not require negative gate-source voltages to operate. Dedicated switching networks are included in the rectifiers' dc paths, to assist branches' activations/deactivation by modifying the rectifiers' dc loads.

The chosen topology is modular and allows to increase the number of branches in a straightforward way if a higher dynamic range is needed. Starting from the idea of the three-branch rectifier presented in [14], this work expands the overall dynamic range of the system up to 45 dB and the

validates the prototype performance by means of a vast experimental campaign. In particular, they include measurements of the return loss at system input port, open-circuit measurements at the dc outputs, over the entire system operating range to demonstrate the exploitation of the cascaded rectifiers in scenarios with unpredictable incoming power.

The paper is organized as follows. In Section II, the design of the cascaded rectifiers is described, followed by the description of the switching network. The validation measurements are proposed in Section III, where the overall system performance are discussed, including those related to the switches. Section IV draws the conclusions.

II. THE MODULAR RECTIFIER DESIGN

The circuit schematic of the proposed modular rectifier is shown in Fig.1. It consists of three rectifiers connected in parallel: in the first design step, they have been designed separately and their performances in terms of RF-to-dc conversion efficiency and dc-voltage have been optimized for a selected power range, covering all together a 45-dB range from -20 to +24 dBm: the LPR has been optimized to operate in the -20 ÷ 0 dBm range; the MPR one in the 0 ÷ 9 dBm range; the HPR one in the 9 ÷ 24 dBm range. The activation of the appropriate one (and the deactivation of the others) is seamless and takes place through the concurrent operation of switch-based components, controlled two-by-two in a synchronous manner. For each power level higher than 0 dBm, two switches are turned on: one in the RF-path and one in the dc-path. In this way, the following rectifier can exploit all the available input power, while the previous stages have their own load grounded; these zero-Ω-loaded rectifiers undergo a strong mismatch with the source, which involves an almost total reflection of the input power to the branches. Since no branch is placed before the LPR, it includes a switch in the dc path only.

The key phenomena, which the design of the proposed system are based on, are the HEMTs self-biasing and the power-selective nonlinear design of the RF matching networks of the three rectification branches. In particular, the first one allows the activation of a branch with no need for an external bias; the second one, collaborates with the self-biasing mechanism to favor the RF power flow into one branch only, by enhancing input matching and mismatching for a prescribed power range and outside of it, respectively.

The added value, with respect to previous solutions, is the automatic switching, seamlessly driven by the incoming RF power, without the need for control logic and the related energy needs. The HEMTs are operated in floating-gate conditions in such a way that they are turned on by gate self-biasing, resulting from the nonlinearities of the even order. This actuation is enhanced and controlled by the custom design of voltage limiters arranged as the feedback network between the dc output and the HEMT gate terminals.

This results in the realization of a new nonlinear design approach that exploits a concurrent switching mechanism of RF and dc branches.
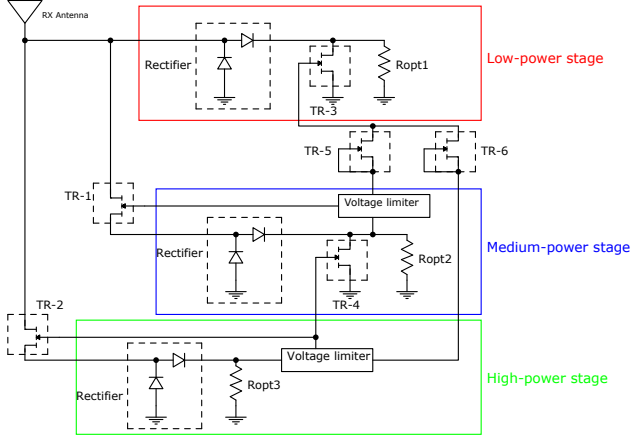
Fig. 1. Schematic of the proposed circuit. Three rectification stages can be observed, and two RF switches (TR-1 and TR-2) are placed in the second and third path, respectively. TR-3 and TR-4 dc switches work in combination of the diverter composed by TR-5 and TR-6, to decouple the first and the second stage.

The HEMTs in the RF paths are normally OFF and isolate the branch they belong to from the rest of the system, when the actual received power value is not suitable for that branch; vice versa they create a conductive path towards the rectification circuit, if the power level is the proper one for that branch. The dc switches perform a complementary action: they are connected in parallel to the dc outputs of the first and second branches and when they are the proper ones the switches are OFF; as soon as they are turned on, they short-circuit the dc loads, thus creating a loading condition far from the optimum one, which results in the reflection of the incoming RF power to the other branches.

A. Seamless RF switching among the rectifiers exploiting HEMTs self-biasing

Usually, in a voltage-controlled RF switch, if the voltage across the gate and source terminals is lower (higher) than the threshold (V_{th}), the transistor behaves as an open (short) circuit. In large-signal regime, the self-polarization phenomenon can be exploited to create dc contributions from the even-order responses [15]. These are exploited in the present system to create the conductive path between the HEMTs drain and source terminals, with no need for an external controlling circuity. This allows a small RF current to flow through the HEMT, hence activating the corresponding rectifier, and consequently the feedback network, which in turn assists in keeping the switch on as long as the input power belongs to the range of that rectifier. The selected HEMT is the Avago ATF-54143, modeled as in [16]. This technique, first proposed in [17] for a two-way rectifier, is modified for the present system for an increased number of rectifier stages to extend the overall dynamic range. In particular, with respect to the work presented in [17], a third stage for high power is added. This allows the increase of the dynamic range from 30 dB up to 45 dB, keeping the RF-to-dc conversion efficiency comparable to the previous version of the work and exploiting the rectification for ultra-low power levels (< -15 dBm).

Moreover, a modular diverter design that enhances the decoupling of multiple branches is presented in this work. The selected switch presents a 36.2 dBm 3rd order intercept and a 20.4 dBm output power at 1 dB gain compression at 2 GHz. Moreover, its threshold voltage and maximum RF input power are typically 0.38 V and 25 dBm, respectively. Exploiting this device, the need for a negative gate voltage is eliminated, which is a typical characteristic of conventional depletion mode devices.

To accurately predict the nonlinear behavior of the switches and their harmonics generation, a harmonic balance (HB) simulation of the HEMT in floating gate conditions has been carried out for different RF excitation levels, namely: -10, 0, and 10 dBm. Fig. 2 shows the static current-voltage (I-V) curve of the HEMT with the superimposed dynamic ones in floating gate conditions, under the different RF excitation conditions.
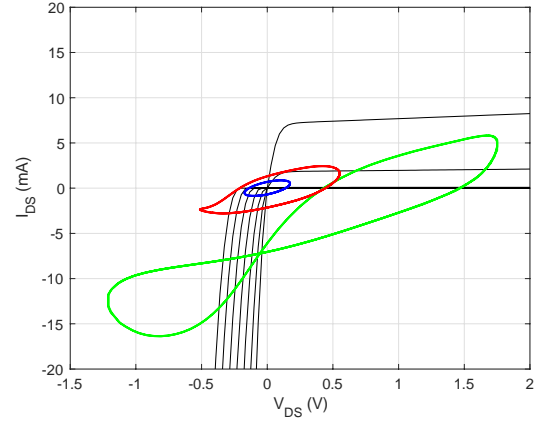

Fig. 2. Static I_{DS}-V_{DS} curve (black) and dynamic load curves of I_{DS} for a RF input power at the drain terminal of -10 dBm (blue), 0 dBm (red) and 10 dBm (green). The self-biasing effect can be seen as the power entering the system increases.

As the RF power increases, the self-polarization effects determine a significant deviation from the corresponding static value of the drain-source current (I_{DS}) dynamic behavior. In particular, it can be observed that the I_{DS} dynamics involve both the first and the third quadrants (see Fig. 2). The smaller closed curve refers to the case of low power (-10 dBm), resulting in an average value of approximately zero and leading to an almost negligible self-polarization effect. While for a 0-dBm RF excitation, corresponding to the red curve, the current shows a slightly non-zero mean value, with a moderate self-biasing effect. Finally, at the highest excitation considered in the analysis (10 dBm), a significant deviation from the zero mean value is retrieved. In this way, the HEMTs (and the related rectifier) are activated as soon as self-biasing causes the voltage across the gate and source terminals to exceed the threshold (V_{th}).

B. Design of the feedback network, the dc switches, and the diverter

Once one rectifier branch is active, the others must be disconnected. For this purpose, two switches are placed in parallel to the first and second output dc-load, TR-3 and TR-4,

respectively (see Fig. 1). As soon as the respective gate-source voltage (V_{GS}) exceeds the threshold, they realize a short-circuit to ground. In this way, the respective rectifiers are driven into operating conditions far from the optimum ones in such a way that their input terminals reflect the incoming RF input power.

For protection purposes of the switches, both the dc and the RF ones, especially in the event of high input power, feedback networks have been introduced at the output of the second and third rectifiers consisting of voltage limiters. They ensure to supply a constant (limited) voltage to the gate terminals of the switches present in the circuit. To achieve this nonlinear functionality, three cascaded diodes and a parallel resistance at the output of the limiters are used. In particular, Skyworks SMS7621 diodes were chosen for the MPR limiter, while Skyworks SMS7630 diodes were adopted for HPR. The circuit schematic of limiters can be found in [17].

The dc switching network, being crossed only by currents with a dc component, consists only of an LC-type low-pass filter on the gate terminal to cancel any residual RF components coming from the feedback network, which can compromise the correct operation of the HEMT.

When the available power exceeds 9 dBm, the HPR is active, disabling the MPR stage. This can cause the deactivation of TR-3, enabling the LPR branch. This twofold undesired effect can cause the failure of the low-power rectifier, due to the exceeding power levels, and thus the overall conversion efficiency degradation. This is solved by adopting the diverter of Fig. 3, consisting of two HEMTs (TR-5 and TR-6), with the gate-drain terminals short-circuited and controlled by the output of the first and second limiters, V_{lim1} and V_{lim2}, respectively.

The diverter circuit enables the HPR and disables the LPR and MPR simultaneously, as soon as the incoming RF power exceeds 9 dBm. Thanks to the controlled polarization of the HEMTs gate terminals, secured by the voltage limiters, as soon as the HPR is activated, the MPR is disabled by forward biasing the gate of TR-4, which also deactivates TR-by short-circuiting the dc output of the MPR.
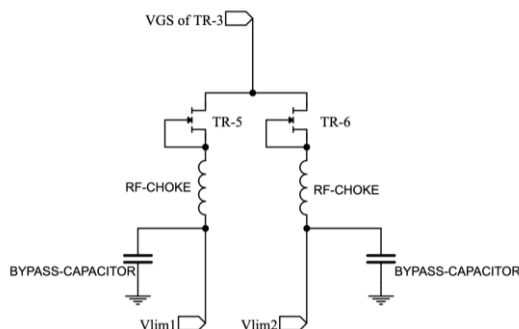

Fig. 3. TR-5 and TR-6 in diverter switch configuration. The gate terminals are shorted to the drain ones to create an input-voltage-controlled HEMT device.

C. Design of the rectifiers

Fig. 4 (a) shows the circuit schematic of the three-branch rectifier arrangement, namely LPR, MPR, and HPR. They all adopt a voltage-doubler rectifier configuration. A T-topology matching network has been optimized for the LPR stage, while for the MPR and HPR ones a double-T structure has

been used to increase the degrees of freedom. The overall power range has been chosen having in mind industrial or civil environments in the presence of RF sources (spontaneous or dedicated) for the wireless power supply of sensors. The choice of three cascaded stages has been driven by the design goal of optimizing the flatness of the rectifiers' RF-to-dc conversion efficiency: being the rectifiers non-linear circuits, each one of them can meet the goal over a limited excitation range. A cascaded architecture allows to select for each branch the most suitable diodes: for increasing input power, diodes with higher breakdown voltage are adopted. It is noteworthy that, due to the modular system of switches, the number of cascaded rectifiers can be increased, for increasing power ranges or for reducing the operating range of each of them. The following Schottky diodes have been selected for the different stages: SMS7630, SMS7621, and HSMS282K diodes have been used for the LPR, MPR and HPR stages, respectively.

The diode voltage-current curve is given by:

$$I = I_s \left(\exp \frac{V}{V_T} - 1 \right) \quad (1)$$

where I_s is the saturation current of the diode and V_T the temperature potential. In Table 1, the main diode parameters such as ideality factor n, breakdown voltage B_V, junction capacitance C_{j0}, and series resistance R_S are shown.

TABLE I
MAIN SPICE PARAMETERS OF THE RF-DIODES

Diode	I_S (A)	n	B_v (V)	C_{j0} (pF)	R_s (Ω)
SMS7630	5e-6	1.05	2	0.14	20
SMS7621	4e-8	1.05	3	0.1	12
HSMS282K	2.2e-8	1.08	15	0.7	6

The system prototype (see Fig. 4 (b)) has been realized on a Rogers RO3003 substrate (thickness: 0.762 mm, ε_r = 3.00). The overall dimension of the prototype is 57 mm x 108 mm but can be further miniaturized by applying meandering techniques [18].

Firstly, the three branches have been optimized separately by means of nonlinear HB simulation, each one for the specific power range of interest, by simultaneously specifying the nonlinear matching (and optimum dc-load) and mismatching, over the power range of interest and outside it, respectively. Then, the full system has been analyzed and a fine tuning of the designable parameters has been carried out leading to the final dimensions reported in Fig. 4 (a).

This design strategy has been able to satisfy the twofold goal of emphasizing the performance of one branch only, in its related power range, and excluding the others by specifying their input mismatch, as well as activating the corresponding dc-networks described in the previous sub-section.

As already mentioned above, this system allows high isolation among the rectifiers branches. This characteristic has been obtained thanks to both the system structure and to the accurate and selective return loss optimization. Large signal S-Parameters (LSSP) are predicted through HB using the software Keysight ADS. In particular, for each branch the

LSSPs has been selectively specified with respect to the input power range, given the highly nonlinear nature of the circuit.

The large signal S_{11} parameters are calculated through the ratio of reflected (b_1) and incident (a_1) wave phasors at the input port and at the fundamental frequency of each stage, where b_1 and a_1 are defined as:

$$b_1 = \frac{1}{2}(\frac{V_{1,1}}{\sqrt{Z_c}} - I_{1,1}\sqrt{Z_c}) \quad (2)$$

$$a_1 = \frac{1}{2}(\frac{V_{1,1}}{\sqrt{Z_c}} + I_{1,1}\sqrt{Z_c}) \quad (3)$$

where $V_{1,1}$ and $I_{1,1}$ are the voltages and currents phasors at the fundamental frequency and at the input ports of the branches and Z_c is the characteristic impedance of the system. Considerable attention has been also given to the behavior of the conversion efficiency (PCE) of the branches: they must maximize the PCE in the respective power ranges of interest, and minimize it elsewhere.

The PCE of each stage is calculated as follows:

$$PCE = \frac{P_{out}}{P_{available}} \quad (4)$$

$$P_{out} = \frac{V_{out}^2}{R_{load}} \quad (5) \quad P_{available} = \frac{V_{av}I_{av}^*}{2} \quad (6)$$

where V_{out}, R_{load}, V_{av}, I_{av} are the dc output voltage, the dc load, the input voltage phasor at the fundamental frequency, respectively.

Both S_{11} and PCE are optimized by HB simulations in such a way that the branches exhibit good performance only in their power range of interest. The optimization objective functions can be summarized as follows:

$$\begin{cases} \max |S_{11}|, \min PCE & outside \; P_{av} \; correct \; range \\ \min |S_{11}|, \max PCE & inside \; P_{av} \; correct \; range \end{cases} \quad (7)$$

III. VALIDATION MEASUREMENTS

This section is dedicated to the experimental characterization of the system of rectifiers. It is noteworthy that the adopted rigorous nonlinear design method described in the previous section is dependent on the accuracy of the available devices models, including their packages. This justifies quantitative disagreements between simulated and measured results, presented in the following. In particular, a 10% frequency shift has been observed with respect to simulations. Thus, measurements have been carried out accounting for this shift.

A. RF HEMT's transmission coefficient S_{21} characterization

A first characterization of the standalone HEMT under RF excitation has been carried out with variable gate-source bias and the comparison between simulated and measured results is reported in Fig. 5: simulations underestimate the transmission coefficient for $V_{GS} < V_{th}$ (0.5 V). For increasing V_{GS}, a better agreement is observed: in such conditions the transmission coefficient is about -0.8 dB.
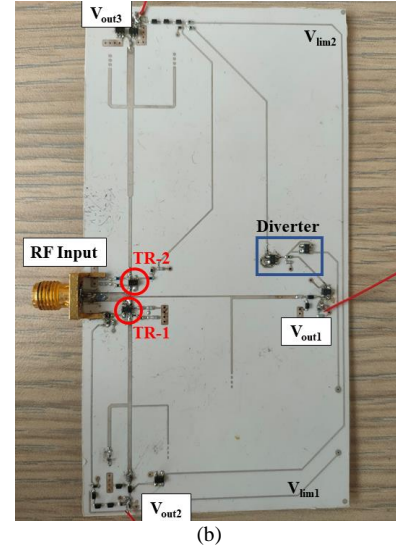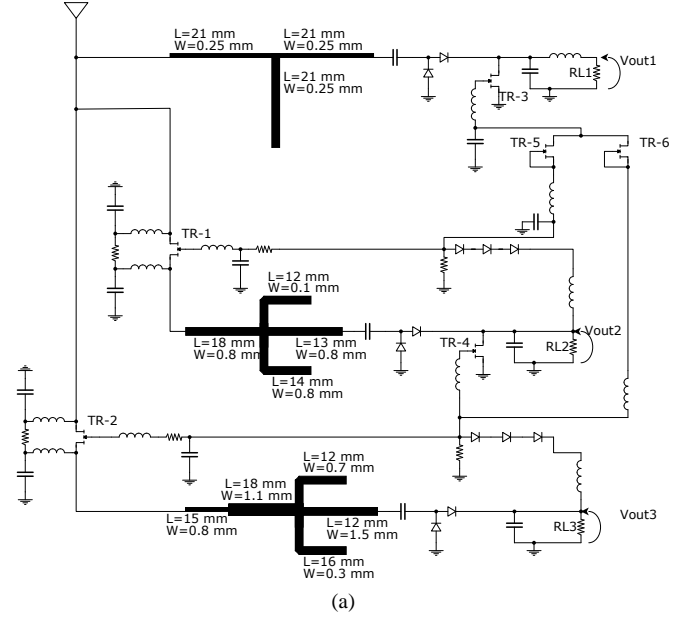

(a)

(b)

Fig. 4. (a) Circuit schematic of the three-branch rectifier and (b) photograph of the fabricated prototype. The three matching networks are visible so the two feeding network which supply the two RF switches (TR-1 and TR-2) and the four dc switches (TR-3, TR-6 and finally the diverter composed by TR-5 and TR-6).

B. Measurement of the three-stage reflection coefficient

In Fig. 6(a) the simulated S_{11} parameter of each stage is with respect to input power. Through a power-selective S_{11} parameter optimization, each branch exhibits a return-loss coefficient higher than 20 dB in its proper power range, and an almost complete reflection of the incident power outside the operating range. As already mentioned in Section II.B, the diverter and switches separate each stage from the others thanks to the self-biasing effect and the feedback network. When the input level is in the low-power range, the second and the third stages act as open circuits, offering an almost infinite impedance, and only the first branch offers a favorable return loss such that a good matching is obtained. When the

medium or the third stage are active, the low-power one is inhibited thanks to TR-3. In this way, a dynamic matching/mismatching of the low-power branch is performed.

Using a vector network analyzer (VNA), the reflection coefficient of the entire system (S_{sys}) hs been measured in large signal conditions, from -20 dBm up to 10 dBm (upper limit of the instrument) and is reported in Fig. 6 (b) together with the simulated results of the entire system and of each branch: it can be seen that the system reflection coefficient is below -10 dB almost over the entire measured power range. A higher S_{sys} parameter is observed when the second branch is turned on and assumes values well below -10 dB after the transition from one stage to another.
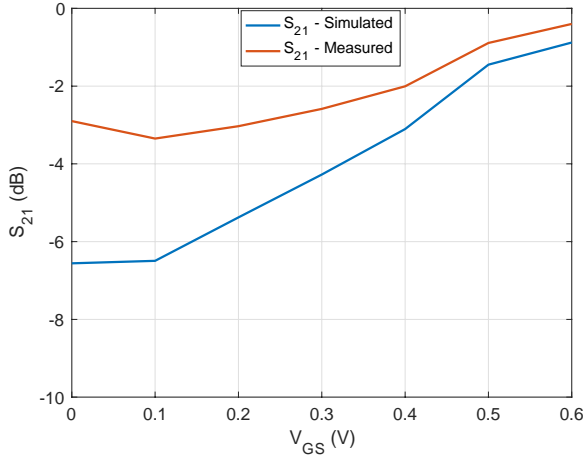

Fig. 5. Simulated and measured transmission coefficient of the standalone RF HEMT switches at the first harmonic.
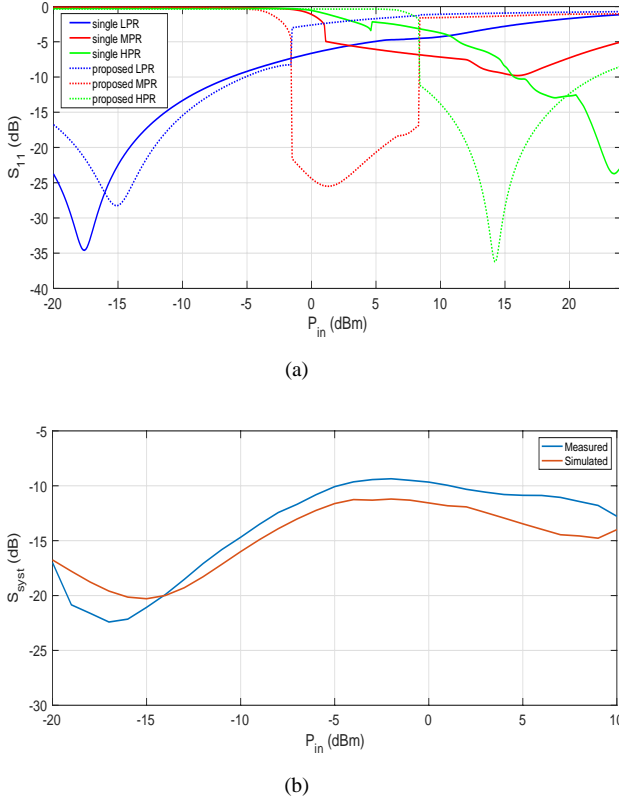

(a)

(b)

Fig. 6. Simulated and measured S_{11} parameters of each branch as the input power varies (a). Reflection coefficient of the entire system in the measured power range (b): it results below -10 dB for most of the interval.

C. Dc open-circuit voltage measurements and optimum load tuning

As a further test, the dc output of each rectifier stage has been evaluated in open circuit voltage conditions.

This has been done to provide the overall evaluation of the system, and to verify the optimum loading conditions, corresponding to the halved open-circuit-voltage [16].
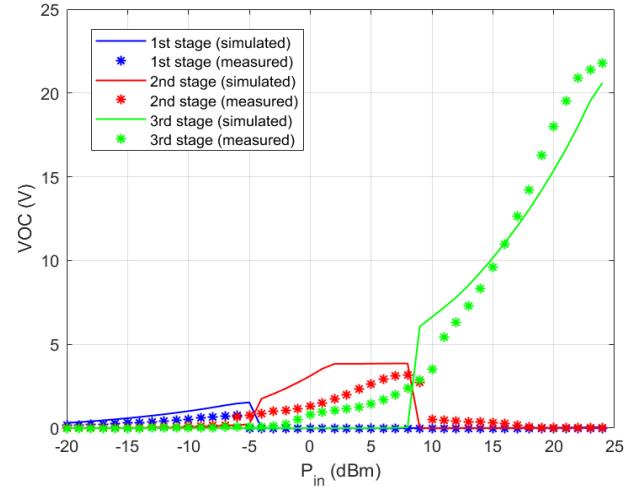

Fig. 7. VOC at the output of each stage. Solid lines represent simulated values, whereas dots are the measured values for different input powers.

Fig. 7 reports the measured dc open circuit voltage (VOC) at each rectifier output. It is worth noticing that, in such loading conditions too, where the loads are disconnected, the switching among the three rectifiers takes place.

Subsequently, a set of measurements has been carried out varying the dc load of the LPR and of the MPR, at P_{in} equal to -10 dBm and 5 dBm, respectively, starting from the optimum load value established during the optimization procedure. Fig. 8 report the behavior of PCE as a function of the load, for the LPR, MPR, and HPR branches.
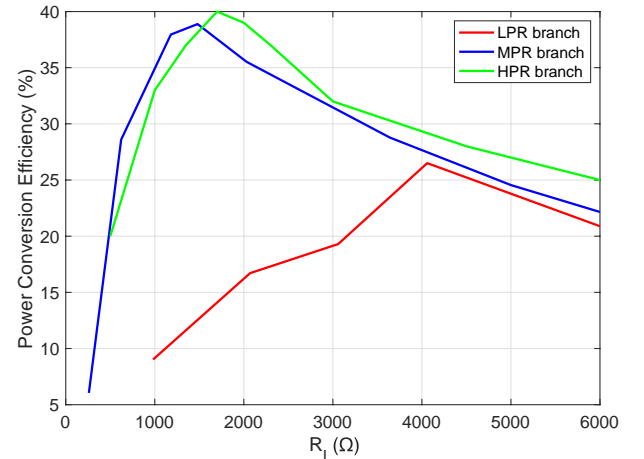

Fig. 8. Behavior of PCE with respect to the loads (R_{L1}, R_{L2} and , R_{L3}) placed at the output of the rectifiers branches.

Here, it is possible to see that the PCE is maximized for a specific value of the load, i.e., R_{L1} = 4.06 kΩ and R_{L2} = 1.48 kΩ, for the first and the second stage, respectively. For these tests, an input power of -10 and 5 dBm have been adopted for the LPR and MPR branches, respectively, achieving a PCE of 26.5% for the first stage and of 38.9% for the second one. Load tuning analysis has been conducted for the third stage, and the best value turned out to be R_{L3} = 1.73 kΩ as predicted by HB simulations.

This has been done to emulate the behavior of the maximum power point tracker (MPPT), a base-band sub-system included in most of the PMUs reported in the literature. The use of multiple loads for the proposed multi-stage rectifier has been chosen to maximize the RF-to-dc conversion operation with respect to single-load solutions proposed in the literature. In particular, to the authors' knowledge the proposed approach turns out to be the only one capable of working efficiently over a very large power range, starting from ultra-low power levels. A 20% power conversion efficiency at -20 dBm is demonstrated, resulting in a dc output power of approximately 2 µW. Indeed, efficient exploitation of a multiple-load rectifier is made possible in conjunction with the use of multi-input PMUs, whose architectures have been already proved by many authors with both off-the-shelf components and dedicated ASICs [19-20]. PMUs capable of controlling the DC output voltage, starting from multiple inputs, enable the concurrent use of largely different input power levels. To comply with the lowest harvestable powers, conversion circuits with a low leakage current have been demonstrated. Usually, they require a minimum input power, for the start-up phase, approximately as low as 1 µW [21]. Conversely, single-stage converters, suitable for solutions with shared load between the various rectifier stages, usually require a minimum start-up power of 100 µW. Thus, adopting a single-load choice may result in an unnecessary inhibition of the overall system operations (rectifier and PMU) in ultra-low power conditions, causing an harvested dc power below the minimum switch-on threshold of the PMU.

Through the fractional open-circuit voltage (FOCV) technique available in many recent PMUs [22], it is possible to adjust the rectifier output voltage to ensure the MPPT, by the continuous tracking of the open-circuit voltage at the rectifiers outputs. This has been demonstrated for voltage variations similar to the ones addressed by the present work (see Figs: 9 (a) and (b)), namely from 0.1 V to 12.5 V for RF inputs of -20 dBm and + 24 dBm, respectively. Such wide voltage range is covered by multi-stage PMUs adopting different CMOS process technologies, capable of extending the PMUs operating range at input voltages exceeding 10 Volts. In particular, by the Bipolar-CMOS-DMOS (BCD) technology, a single integrated converter can be adopted for low- and high-power regimes. Another option can be to regulate the input voltage adopting level-shifter circuits resulting in improved dc-dc efficiencies [23]. Thus, using a multi-load rectification system not only allows to maximize the RF-to-dc conversion efficiency, for any RF input power over a very large range, but also is suitable in conjunction with multi-input PMUs.

D. Results of measured PCEs with different sweeping power configurations

In realistic IoT scenarios, the system may be closer to and further from the RF source over time, and its seamless switching capabilities must be tested for both increasing and decreasing the available power. For this purpose, to verify the ON/OFF switching capabilities of the proposed system, measurements have been performed with the optimal loads mimicking a PMU placed downstream of the circuit.

Figs. 9 and 10 report the measured results for increasing and decreasing available power, respectively. Both the dc voltage and the PCE are shown. The measured and simulated curve trends are in good agreement especially as regards the switching mechanisms among rectifiers and the resulting behaviors of both the dc voltage and the PCE. Quantitative differences between the measured and simulated values are observed: in particular, a frequency shift, of about 200 MHz has been measured and, consequently, an efficiency offset of about 10% has been obtained. These dissimilarities may be due to inaccuracies of the components' models available for the simulations, in particular the models for the HEMT-based switches, whose measured insertion loss resulted to be higher than the predicted ones. A more accurate model of the nonlinear device may fill this gap because of a better description of the nonlinear input impedance, crucial for the present design. A dedicated characterization of the decoupling network subsystem has been carried out and resulted in an excellent agreement with simulations. This is indirectly confirmed in Fig. 9 and Fig. 10 by observing that input power levels driving the first stage turn-off (and turn-on of the second stage) is 0 dBm, while a 2-dB shift is noticed in the deactivation/activation phase of the second/third stage.

On the overall, it can be stated that the idea proposed in this work is a suitable candidate for energy harvesting in IoT environments where a battery-less sensor node has to deal with unknown available RF power occurrence.

TABLE II
COMPARISON OF WIDE DYNAMIC RANGE EH SOLUTIONS

Work	Frequency [GHz]	RF Power Input (dBm)	Dynamic Range (dB)	20% PCE @ (dBm)	Power Distribution Technique	Need for external control
[8]	2.3-2.45	5 to 45	40	9	SPDT switches with controller and power monitor	Yes
[9]	0.9	- 4 to 25	29	-7	Adaptive matching design	No
[10]	2.4	- 10 to 30	40	-10	Adaptive matching design	No
[11]	2.4	-10 to 30	40	-10	Adaptive matching design	No
[12]	2.27	-20 to 25	45	-16	Power divider and HEMT rectifiers	No
This work	2.26	-20 to 24	44	-20	Adaptive matching design and passive HEMT switches	No

Table II reports a comparison among the solutions available in the literature and the outcome of this work. Operating frequency, power range, power distribution techniques and the major performance indicators are reported. The proposed solution spans a 45-dB power range that is, according to the authors' knowledge, among the largest ones for RF-to-dc converters available in the literature especially power levels as low as -20 dBm are addressed.
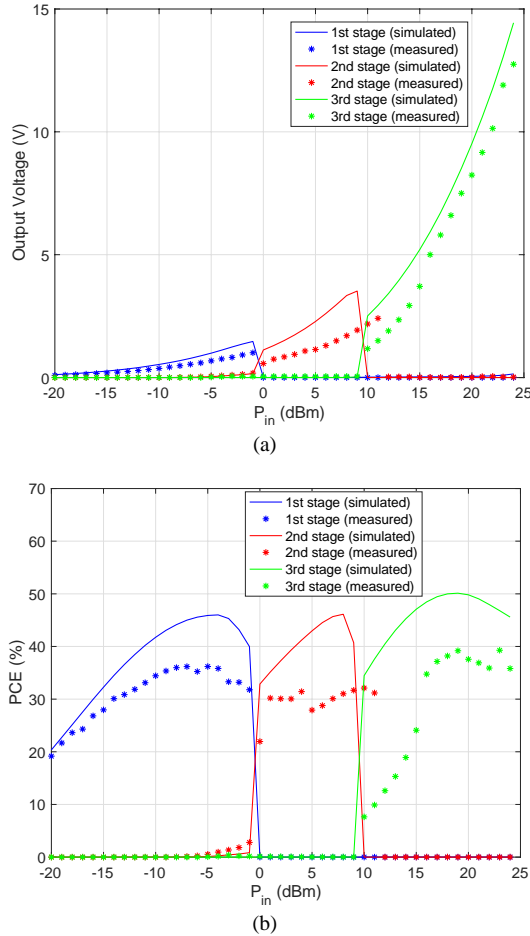

(a)

(b)

Fig. 9. Simulated (solid lines) and measured (dots) values of (a) output voltage V_{OUT} and (b) RF-to-dc PCE for the three stages measured with RF input power going from -20 to 24 dBm at 2.26 GHz (forward P_{in} sweep).
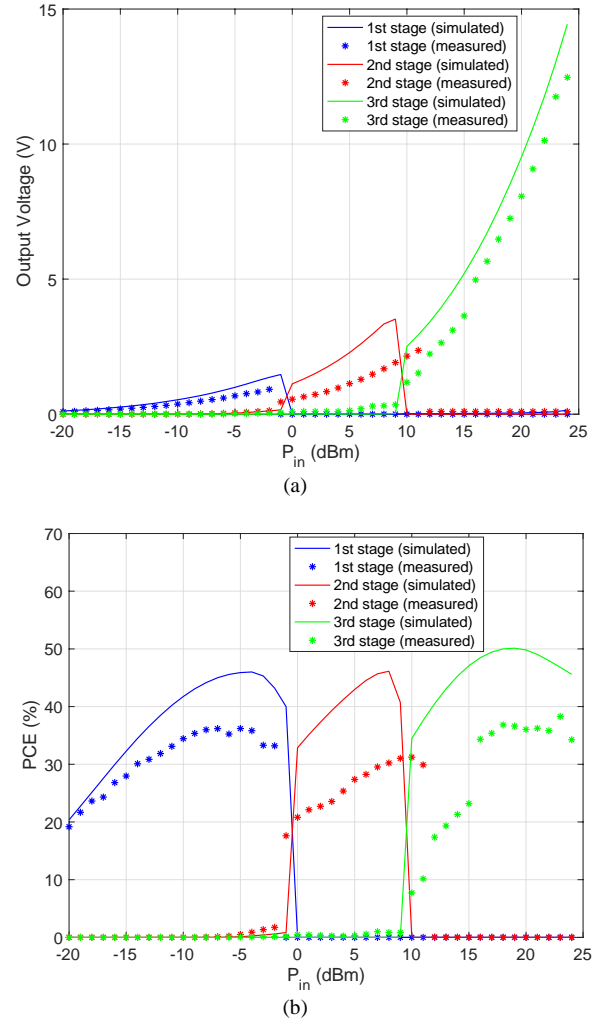

(a)

(b)

Fig. 10. Simulated (solid lines) and measured (dots) values of (a) output voltage V_{OUT} and (b) RF-to-dc PCE for the three stages measured with RF input power going from 24 to -20 dBm at 2.26 GHz (backward P_{in} sweep).

IV. CONCLUSION

This work has presented the design and characterization of an innovative architecture of rectifiers alternatively turned on and off, depending on the input power range. It occurs

seamlessly with no need for external and power-consuming control. The goal of these cascaded rectifiers is to ensure a large dynamic range, starting from ultra- low power levels so that they can be adopted on board of battery-less sensors for IoT applications. In particular, the present version of the system operates from -20 dBm to 24 dBm, but it can be extended by increasing the number of cascaded rectifiers. Compared to solutions previously presented in the literature, the proposed one is the only one able to work at extremely low powers, with a 20% RF-to-dc conversion efficiency at -20 dBm. Such performance has been obtained by adopting a novel nonlinear design of the rectifiers matching networks, to be selective with respect to the incoming power range, combined with the design of a system of dc switches, to create a strong decoupling between the rectifiers. Measurements have confirmed that the system can switch on the proper rectifiers bidirectionally, for both increasing and decreasing input power with stable performance, without the need for an external control circuit, because is the system itself that is able to auto-select the proper rectifier branch.

REFERENCES

[1] H. Hayashi and T. Ueda, "Requirements and considerations of energy harvesting for industrial wireless transmitter," in *Proc. of SICE Annual Conf. (SICE)*, 2012, pp. 1414-1415.
R. Correia, N. Borges Carvalho and S. Kawasaki, "Continuously Power Delivering for Passive Backscatter Wireless Sensor Networks," in *IEEE Trans. Microw. Theory Techn*, vol. 64, no. 11, pp. 3723-3731, Nov. 2016.

[2] S. Kim *et al.*, "Ambient RF Energy-Harvesting Technologies for Self-Sustainable Standalone Wireless Sensor Platforms," in *Proc. of the IEEE*, vol. 102, no. 11, pp. 1649-1666, Nov. 2014.

[3] C. Viehweger, T. Keutel, and O. Kanoun, "Energy harvesting for wireless sensor nodes in factory environments," in *IEEE 11th Intern. Multi-Conf. on Syst., Signals & Devices (SSD14)*, 2014, pp. 1-4.

[4] F. Deng, X. Yue, X. Fan, S. Guan, Y. Xu, and J. Chen, "Multisource Energy Harvesting System for a Wireless Sensor Network Node in the Field Environment," in *IEEE Internet Things J.*, vol. 6, no. 1, pp. 918-927, Feb. 2019.

[5] T. Kavitha and S. Silas, "A Survey on Energy Harvesting Routing Protocol for WSN," in *3rd Intern. Conf. on Trends in Electronics and Informatics (ICOEI)*, 2019, pp. 572-575.

[6] M. Sansoy, A. S. Buttar, and R. Goyal, "Empowering Wireless Sensor Networks with RF Energy Harvesting," in *7th Intern. Conf. on Signal Processing and Integrated Networks (SPIN)*, 2020, pp. 273-277.

[7] G. Paolini, M. Feliciani, D. Masotti, and A. Costanzo, "Toward an Energy-Autonomous Wearable System for Human Breath Detection," in *IEEE MTT-S Intern. Microw. Biomedical Conf. (IMBioC)*, 2020, pp. 1-3.

[8] S. Yoshida, G. Fukuda, T. Noji, S. Tashiro, Y. Kobayashi, and S. Kawasaki, "Wide power range operable 3-stage S-band microwave rectifier with automatic selector based on input power level," in *IEEE MTT-S Intern. Microw. Symp. Digest (MTT)*, 2013, pp. 1-4.

[9] X. Wang and A. Mortazawi, "Rectifier Array With Adaptive Power Distribution for Wide Dynamic Range RF-DC Conversion," in *IEEE Trans. Microw. Theory Techn*, vol. 67, no. 1, pp. 392-401, Jan. 2019.

[10] P. Wu, Y. Chen, W. Zhou, Z. H. Ren, and S. Y. Huang, "A Wide Dynamic Range Rectifier Array Based on Automatic Input Power Distribution Technique," in *IEEE Microw. Wireless Compon. Lett.*, vol. 30, no. 4, pp. 437-440, April 2020.

[11] S. Y. Zheng, S. H. Wang, K. W. Leung, W. S. Chan, and M. H. Xia, "A High-Efficiency Rectifier With Ultra-Wide Input Power Range Based on Cooperative Structure," in *IEEE Trans. Microw. Theory Techn*, vol. 67, no. 11, pp. 4524-4533, Nov. 2019.

[12] J. Yamazaki, R. Ishikawa, and K. Honjo, "Input-Power-Synchronous Adaptively Biased Wide-Dynamic-Range High-Efficiency Rectifier with Zero-Threshold GaAs HEMTs," in *50th European Microw. Conf. (EuMC)*, 2021, pp. 436-439.

[13] H. Ishida *et al.*, "A high-power RF switch IC using AlGaN/GaN HFETs with single-stage configuration," in *IEEE Trans. Electron. Devices*, vol. 52, no. 8, pp. 1893-1899, Aug. 2005.

[14] S. Trovarello, G. Paolini, D. Masotti and A. Costanzo, "A Modular System of Rectifiers for Energy Harvesting with Wide Dynamic Input-Range," in *6th International Conference on Smart and Sustainable Technologies (SpliTech)*, 2021, pp. 1-4.

[15] H. Abe, "A GaAs MESFET Self-Bias Mode Oscillator (Short Paper)," *IEEE Trans. Microw. Theory Techn*, vol. 34, no. 1, pp. 167-172, Jan 1986.

[16] W. R. Curtice, "A MESFET Model for Use in the Design of GaAs Integrated Circuits," in IEEE *IEEE Trans. Microw. Theory Techn*, vol. 28, no. 5, pp. 448-456, May 1980.

[17] M. Del Prete, D. Masotti, and A. Costanzo, "Automatically switchable two-way rectifier," in *50th European Microw. Conf. (EuMC)*, 2021, pp. 440-443.

[18] D. Masotti, A. Costanzo, P. Francia, M. Filippi, and A. Romani, "A Load-Modulated Rectifier for RF Micropower Harvesting With Start-Up Strategies," in *IEEE Trans. Microw. Theory Techn*, vol. 62, no. 4, pp. 994-1004, April 2014.

[19] S. S. Amin and P. P. Mercier, "MISIMO: A multi-input single-inductor multi-output energy harvester employing event-driven MPPT control to achieve 89% peak efficiency and a 60,000x dynamic range in 28nm FDSOI," 2018 IEEE International Solid - State Circuits Conference - (ISSCC), 2018, pp. 144-146.

[20] A. Abuellil, J. J. Estrada-López, A. Bommireddipalli, A. Costilla-Reyes, Z. Zeng and E. Sánchez-Sinencio, "Multiple-Input Harvesting Power Management Unit With Enhanced Boosting Scheme for IoT Applications," in IEEE Transactions on Industrial Electronics, vol. 67, no. 5, pp. 3662-3672, May 2020.

[21] K. Kadirvel, Y. Ramadass, U. Lyles, J. Carpenter, V. Ivanov, V. McNeil, A. Chandrakasan, and B. Lum-Shue-Chan, "A 330nA energy-harvesting charger with battery management for solar and thermoelectric energy harvesting," in Proc. IEEE Int. Solid-State Circuits Conf., Feb. 2012, pp. 106–108.

[22] M. Dini, A. Romani, M. Filippi, V. Bottarel, G. Ricotti and M. Tartagni, "A Nanocurrent Power Management IC for Multiple Heterogeneous Energy Harvesting Sources," in IEEE Transactions on Power Electronics, vol. 30, no. 10, pp. 5665-5680, Oct. 2015.

[23] D. Masotti, A. Costanzo, P. Francia, M. Filippi and A. Romani, "A Load-Modulated Rectifier for RF Micropower Harvesting With Start-Up Strategies," in IEEE Transactions on Microwave Theory and Techniques, vol. 62, no. 4, pp. 994-1004, April 2014.

Simone Trovarello (Student Member, IEEE) received the M.Sc. degree in electronics and telecommunications engineering from the University of Bologna, Bologna, Italy, in 2020. In 2021, he joined the Department of Electrical, Electronic and Information Engineering "G. Marconi" (DEI), University of Bologna as a Research Fellow with the EU project "NANO-EH". He is currently a PhD Student in electronics, telecommunications, and information technologies engineering. His research interests include energy harvesting at microwaves and mm-waves, ferroelectric materials for beam-steering applications and integration on silicon of RF devices.

Giacomo Paolini (Member, IEEE) received the M.Sc. degree in biomedical engineering and the Ph.D. degree in electronics, telecommunications, and information technologies engineering from the University of Bologna, Bologna, Italy, in 2016 and 2021, respectively. In 2016, he joined the Interdepartmental Center for Industrial ICT Research (CIRI

ICT), University of Bologna, as a Research Fellow with EU-supported "HABITAT" Project. He is currently a Postdoctoral Researcher with the Department of Electrical, Electronic and Information Engineering "G. Marconi" (DEI), University of Bologna. His research interests include microwave radar systems for biomedical applications, indoor positioning exploiting RFID technologies, and far-field wireless power transfer systems.

Diego Masotti (Senior Member, IEEE) received the Ph.D. degree in electric engineering from the University of Bologna, Italy, in 1997. In 1998, he joined the University of Bologna and is currently an Associate Professor of electromagnetic fields. He authored more than 70 scientific publications on peer reviewed international journals and more than 130 scientific publications on proceedings of international conferences. His research interests include nonlinear microwave circuit simulation and design, with emphasis on nonlinear/electromagnetic co-design of integrated radiating subsystems/systems for wireless power transfer and energy harvesting applications. Dr. Masotti is serves in the Editorial Board of the International Journal of Antennas and Propagation, Journal of Wireless Power Transfer, IEEE ACCESS, and Electronics Letters, and is a Member of the Paper Review Board of the main Journals of the microwave sector.

Alessandra Costanzo (Fellow, IEEE) is currently a Full Professor with the Alma Mater Studiorum, University of Bologna, Cesena, Italy. She has authored more than 260 scientific publications in peer-reviewed international journals and conferences and several chapter books. Recently, she has proposed novel solutions for energy-autonomous RF systems based on the wireless power transmission, adopting both far-field and near-field solutions, for several power levels and operating frequencies. Her current research interests include CAD algorithms for multi-domain co-design and modeling of active nonlinear microwave/RF circuits. Dr. Costanzo is a Member of the MTT-24 Committee on Radio Frequency Identification (RFID). She is the Past-Chair of the MTT-26 Committee on Wireless Energy Transfer and Conversion and has been the TPC Co-Chair of MTT-S WPTC2019. Since 2016, she has been the Steering Committee Chair of the IEEE JOURNAL OF RADIO FREQUENCY IDENTIFICATION. She is a past Associate Editor for the IEEE TRANSACTIONS ON MICROWAVE THEORY AND TECHNIQUES, an Associate Editor for the Cambridge International Journal of Microwave and Wireless Technologies. She is a Co-Founder of the EU COST Action IC1301 WiPE Wireless Power Transfer for Sustainable Electronics. She is the MTT-S Representative and

a Distinguished Lecturer of the Council on Radio Frequency Identification (CRFID). In November 2021, she has been elevated to IEEE Fellow, effective January 2022 with the following citation: "for contributions to nonlinear electromagnetic co-design of RF and microwave circuits".